Chinese Journal of
POLYMER SCIENCE

ARTICLE

https://doi.org/10.1007/s10118-018-2016-z
Chinese J. Polym. Sci. 2018, 36, 78–84

Random Binary Brush Architecture Enhances both Ionic Conductivity and Mechanical Strength at Room Temperature

Yu-Feng Lyu[a†], Zhi-Jie Zhang[b†], Chang Liu[b], Zhi Geng[a], Long-Cheng Gao[a*], and Quan Chen[b*]

[a] *Key Laboratory of Bio-inspired Smart Interfacial Science and Technology of Ministry of Education, School of Chemistry and Environment, Beihang University, Beijing 100191, China*
[b] *State Key Laboratory of Polymer Physics and Chemistry, Changchun Institute of Applied Chemistry, Chinese Academy of Sciences, Changchun 130022, China*

Electronic Supplementary Information

Abstract The ionic conductivity and the mechanical strength are two key factors for the performance of poly(ethylene oxide) (PEO) based polyelectrolytes. However, crystallized PEO suppresses ion conductivity at low temperature and melted PEO has low mechanical strength at high temperature. Here, random binary brush copolymer composed of PEO- and polystyrene (PS)-based side chains is synthesized. PEO crystallinity is suppressed by the introduction of PS brushes. Doping with lithium trifluoromethanesulfonate (LiTf) induces microphase separation. Due to a random arrangement of the brushes, the microphase segregation is incomplete even at high salt loading, which provides both high ionic conductivity and high mechanical strength at room temperature. These results provide opportunities for the design of polymeric electrolytes to be used at room temperature.

Keywords Binary brush copolymer; PEO; Ionic conductivity; Phase separation

Citation: Lyu, Y. F.; Zhang, Z. J.; Liu, C.; Geng, Z.; Gao, L. C.; Chen, Q. Random Binary Brush Architecture Enhances both Ionic Conductivity and Mechanical Strength at Room Temperature. Chinese J. Polym. Sci. 2018, 36(1), 78–84.

INTRODUCTION

Polymer membranes with high ionic conductivity have attracted intense interests during the past decade due to their promising energy-related applications[1, 2]. Since the development of the first "dry solid" polymer electrolyte[3], poly(ethylene oxide) (PEO) has become the most employed polymer as electrolyte of rechargeable lithium ion batteries[4–11]. Unfortunately, a high degree of crystallinity in PEO limits the ions transport at temperature below the melting point[12–14].

In addition to the ionic conductivity, the mechanical performance is of particular importance. The low mechanical strength of PEO homopolymer often causes the dendrite problem, an inherent safety challenge for all lithium-based batteries[15, 16]. PEO based polymeric electrolytes with high ionic conductivity and high mechanical stability can be achieved with phase-separated nanostructures, where one phase conducts ions and the other provides mechanical support. However, the crystalline problem still remains with PEO of high molecular weight. Balsara and coworkers designed microphase-separated block copolymer composed of PEO and polystyrene (PS), for which the high storage modulus of 0.1 GPa appeared to effectively suppress the dendrite growth. However, the semicrystallinity structure of PEO phase limited the ion transport[16, 17]. In summary, it is appealing to have microphase-separated structures containing ion-conducting PEO phase and mechanical supporting phase. For PEO phase, the spatial continuity is preferred in promoting the ion conduction[18, 19], while the crystallinity is not[20, 21]. Moreover, several other structural factors, including the orientation of the conducting nanochannels, the defects between the conducting domains, influence also the conductivity dramatically.

In respect to the points mentioned above, we explore binary and random brush copolymers (BBCP) with PEO of low molecular weight and PS side chains, both randomly grafted onto one backbone (Fig. 1). The BBCP copolymer is different from block copolymer in two aspects. First, the random arranged branches are difficult to segregate completely. Second, the segregation, if occurs, is most likely along the main backbone[22, 23]. Considering a steric crowding of densely grafted side chains, the backbone is usually non-flexible. Therefore, it is unlikely for random BBCP to segregate into microstructure with highly curved surface. It turns out that the short PS and PEO brushes are miscible at molecular scale in BBCP. Nevertheless, salt-induced microphase separation occurs after doping with lithium trifluoromethane sulfonate (LiTf). Due to the random arrangement of the side chains, the phase segregation is not complete even at high salt loading, allowing PEO to be amorphous at all temperature examined.

* Corresponding authors: E-mail lcgao@buaa.edu.cn (L.C.G.)
E-mail qchen@ciac.ac.cn (Q.C.)
† These authors contributed to this work equally.
Received June 26, 2017; Accepted August 2, 2017; Published online October 30, 2017

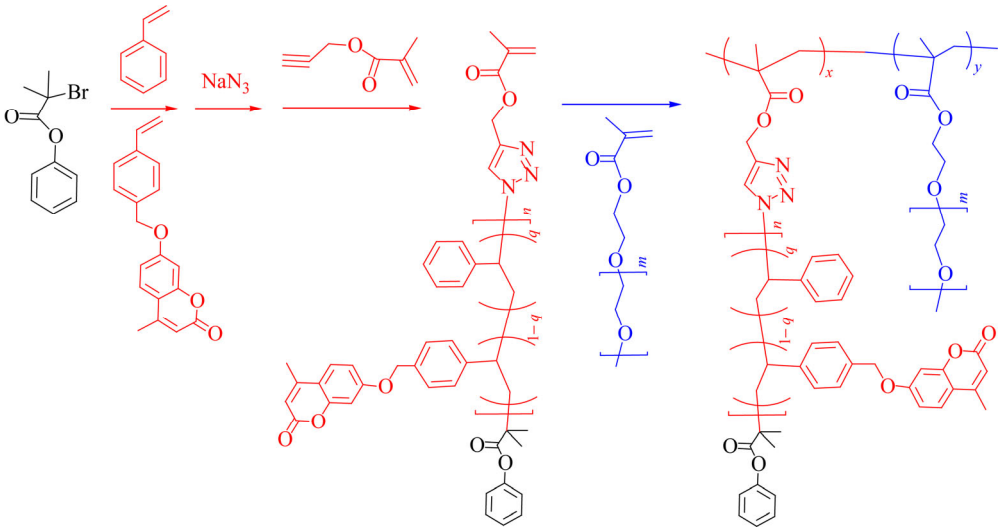

Fig. 1 Synthesis procedure of BBCP

EXPERIMENTAL

Materials

Chlorobenzene and THF (analytical purity, Beijing Chemical Reagents Co.) were refluxed with powdered CaH_2 and distilled. CuBr was synthesized in our lab from $CuBr_2$[24]. 7-Hydroxyl-4-methylcoumarin (analytical purity, Beijing Chemical Reagents Co.), *N*,*N*,*N*′,*N*″,*N*‴-pentamethyl-diethylenetriamine (PMDETA, 98%, Adamas-beta), 1-(chloromethyl)-4-vinylbenzene (97%, Aldrich), propargyl alcohol (analytical purity, Beijing Chemical Reagents Co.), methacrylic acid (analytical purity, Beijing Chemical Reagents Co.), 2-((phenylcarbonothioyl)thio)acetic acid (99%, J&K), 1-ethyl-3-(3-dimethylaminopropyl)carbodiimide hydrochloride (EDC, analytical purity, Beijing Chemical Reagents Co.), and 4-dimethylaminopyridine (4-DMAP, 97%, Heowns) were used as received. Styrene (analytical purity, Beijing Chemical Reagents Co.) was purified under reduced pressure distillation. In order to remove the inhibitor, oligo(ethylene glycol) methyl ether methacrylate (OEGMA, M_n = 950, Aldrich) was passed through a short basic alumina column. Other agents were used as received except otherwise described. PS-N_3 was synthesized according to a reported work[25].

Synthesis of Propargyl Methacrylate

Into a flask of 500 mL, 10.0 g of propargyl alcohol (0.18 mol), 15.4 g of methacrylic acid (0.18 mol), 68.4 g of EDC (0.36 mol), 2.2 g of 4-DMAP (0.018 mol) and 250 mL of CH_2Cl_2 were added. The reaction was allowed for 2 days at room temperature. Then the mixture was washed with water for 3 times, and the combined organic phase was dried by $MgSO_4$. The pure product was obtained by column separation with CH_2Cl_2/petrol ether (1/1, *V*/*V*) as the eluent (12.9 g, yielding 58%). ^{1}H-NMR (400 MHz, $CDCl_3$, TMS, δ, ppm): 6.21 (s, 1H, =C<u>H</u>H), 5.64 (s, 1H, =CH<u>H</u>), 4.75 (s, 2H, C<u>H</u>$_2$O), 2.48 (s, 1H, CC<u>H</u>), 1.96 (s, 3H, C<u>H</u>$_3$).

Synthesis of PS Macromonomer

PS macromonomer was synthesized by click chemistry. 5.3 g of PS-N_3 (1.82 mmol) was dissolved in 20 g of THF, followed by addition of 0.3 g of propargyl methacrylate (2.42 mmol), 80 mg of PMDETA (0.46 mmol) and 50 mg of CuBr (0.35 mmol). The mixture was degassed by three freeze-pump-thaw cycles, and sealed under vacuum. The reaction tube was placed in ambient environment for 72 h. The mixture was diluted with CH_2Cl_2, passed through a basic alumina column, precipitated into methanol. The product was filtered and dried under vacuum, yielding the PS macromonomer. The chemical structure was confirmed by GPC and ^{1}H-NMR, as shown in Figs. S1–S3 (in electronic supplementary information, ESI).

Synthesis of BBCP

PS macromonomer (3.4 g, 1.17 mmol) and 1.7 g of OEGMA were first dissolved in 20 g of chlorobenzene, and 10 mg of AIBN (0.06 mmol) and 25 mg of 2-((phenyl-carbonothioyl) thio)acetic acid (0.02 mmol) were added into the solution. The mixture was degassed by three freeze-pump-thaw cycles, and sealed under vacuum. The reaction tube was placed in an oil bath at 60 °C for 41 h. The polymerization was quenched by dipping the tube in ice/water and the tube was broken to get the sample. The mixture was diluted with CH_2Cl_2, precipitated into cold petrol ether. With the solvent removed, the raw product was washed with methanol to remove the OEGMA macromonomer. After methanol was removed, the sample was dried in vacuum and then dissolved in CH_2Cl_2 and the solution was passed through a silica gel column with acetone as the eluent, yielding the pure BBCPs (1.0 g). The molecular weight and polydispersity were determined by GPC ($M_n = 5.72 \times 10^4$, PDI = 1.41, shown in Fig. S4, in ESI). The composition was calculated from ^{1}H-NMR (weight fraction of PEO: w_{PEO} = 46.8%, PS macromonomer conversion: 15.6%; OEGMA conversion: 27.5%).

Measurements

The number-average molecular weights (M_n) and molecular weight polydispersity (PDI) of all (co)polymers were measured by gel permeation chromatography (GPC) with a Waters 2410 instrument, which was equipped with three Waters μ-Styragel columns (10^3, 10^4 and 10^5 Å). THF was used as the mobile phase at a flow rate of 1.0 mL/min at 35 °C. The standard curve was obtained by PS standards.

https://doi.org/10.1007/s10118-018-2016-z

The weight fraction of PEO in the BBCPs was obtained from the nuclear magnetic resonance spectroscope (NMR) carried on a Bruker ARX 400MHz spectrometer, in $CDCl_3$ and with tetramethylsilane (TMS) as the reference.

BBCP and various amounts of LiTf were dissolved in THF at concentration of 5 wt%. After solvent annealing under THF atmosphere for 5 days, the samples were dried under vacuum first at 80 °C for three days, and then at 140 °C for one day.

Thermal analysis

Thermal analysis of the polymers and BBCPs/lithium composites was carried out on a TA differential scanning calorimeter (DSC) Q100 calorimeter with a heating rate of 10 K/min and over the temperature range of –80 °C to 200 °C.

Fourier transform infrared (FTIR) spectroscopy

FTIR spectra of the samples were recorded at room temperature using a Bio-Rad FTIR system. The spectra were collected in the range of 600–4000 cm^{-1}.

Small angle X-ray scattering (SAXS)

Small angle X-ray scattering data were obtained at NANOSTAR SAXS system (Bruker AXS). The samples were first annealed at 140 °C for 1 h, and then measured isothermally at every 20 °C steps downwards to room temperature (T). Wide angle X-ray scattering (WAXS) experiment was carried out on the SAXSess high-flux small-angle X-ray scattering instrument (Anton Paar).

Transmission electron microscopy (TEM)

Transmission electron microscopy was used to detect the microphase separation of samples. To enhance the electron density difference between the PS and PEO phases, the PEO domains were preferentially stained by RuO_4 for 3 min at room temperature. TEM studies were carried out on a Hitachi H-800 electron microscope.

Linear viscoelasticity (LVE)

Linear viscoelasticity measurements were conducted on an ARES-G2 rheometer from TA Instruments. Parallel plates with diameters of 8 and 25 mm were used. During the frequency sweep measurement, the diameter parallel plates of 25 mm were used, and strain amplitude was kept in the linear region, as verified by strain amplitude sweeps. During the T sweep measurement, the parallel plates of 8 mm diameter were used. The frequency was kept at $\omega = 1$ rad/s and T was increased at a rate of 1 K/min. For the BBCP bulk sample and samples of lithium-doping ratio (r, defined as the molar ratio between Li and ethylene oxide unit) = 0.05 and 0.1, the T sweep measurement started from 30 °C and ended at high T where $|G^*| < 10^3$ Pa. For the sample of $r = 0.5$, the T sweep measurement started at 60 °C (~10 °C below T_g of the PEO domain) and ended at 220 °C.

Dielectric relaxation spectroscopy (DRS)

Dielectric relaxation spectroscopy measurement was conducted on a Novocontrol GmbH Concept 40 broadhand dielectric spectrometer. Samples were loaded on a freshly polished brass electrode, and heated fast up to 140 °C under vacuum for one day before loading the top brass electrode. Gap size was controlled by placing 0.1 mm silica between the two electrodes. The top electrode was pressed and equilibrated at 140 °C overnight before transferred to the spectrometer. Before the measurement, samples were annealed in the instrument at 140 °C for 1 h under nitrogen for drying. Isothermal frequency sweeps from 10^7 Hz to 10^{-1} Hz were conducted in 10 K steps from 140 °C to –50 °C, with precise temperature control, within ±0.1 K.

RESULTS AND DISCUSSION

Synthetic Procedure

PS macromonomer was synthesized by click chemistry with PS precursor of M_n of 2900 (Fig. S1, in ESI). The transformation of PS-Br into PS-N_3 is quantitatively realized by adding NaN_3. FTIR is used to monitor the procedure by following the typical peak of $-N_3$ group at 2095 cm^{-1} (Fig. S2, in ESI). The PS macromonomer was obtained by click reaction. From the ^{1}H-NMR spectrum, characteristic peaks of acrylic protons are seen at 6.2 ppm (Fig. S3, in ESI). The random brush copolymers was prepared by reversible addition-fragmentation chain transfer polymerization (RAFT) technique. The macromonomers could not reach the full conversion. The remaining OEGMA was washed away with methanol. PS macromonomer was separated by a silica gel column with acetone as the eluent. Compared to traditional fractional precipitation, column separation was fast and of high-yield. From the GPC curve, no macromonomer was detected ($M_n = 5.72 \times 10^4$, PDI = 1.41, Fig. S4 in ESI).

^{1}H-NMR measurement was used to confirm the structures and to calculate chemical composition of BBCPs. ^{1}H-NMR spectrum of BBCP is shown in Fig. S5 (in ESI). The characteristic peaks of the PS block are located in the range of δ from 6.3 ppm to 7.2 ppm. The weight fraction of the POEGMA brush is calculated to be 46.8%.

Morphology

DSC measurement was carried out on macromonomers, their homopolymers and BBCP copolymer, and BBCP doped with LiTf. PEO macromonomer and its brush homopolymer have melting point at low T (32 °C, Fig. S6 in ESI). The PS macromonomer and its brush homopolymer exhibit T_gs of 81 and 96 °C, respectively (Fig. S7, in ESI). As shown in Fig. 2, the glass transition process of BBCP sample is broad and has a two-step profile. The lower and higher T_gs are attributed to PEO and PS brushes, respectively. This feature is typical for miscible polymer pairs with large dynamic asymmetry, which is the case for PS and PEO having more than 100 °C difference in their bulk T_gs. The T_g values of both PEO and PS were different from their homopolymers, attributable to the self-concentration, and further broaden due to the fluctuation of local concentration[26–29]. The random distribution of PEO and PS brushes along the polymer chains suppresses the crystallization of PEO, in contrast to either PEO macromonomer or PEO brush homopolymer that crystalizes at around 32 °C.

After doping with LiTf, salt-induced microphase segregation occurred, owing to the energetically favored PEO/LiTf interaction originated from coordination of Li^+ and PEO segments, resulting in an increase in the effective Flory-Huggins χ parameter between PEO and PS. The lithium salt plays a role similar to a PEO selective solvent[30–33]. In Fig. 2, two distinct T_gs are seen, corresponding to PEO and PS brushes, respectively. Meanwhile, the glass transition gap

https://doi.org/10.1007/s10118-018-2016-z

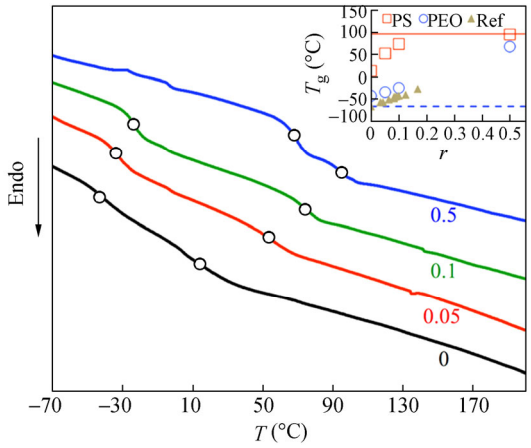

Fig. 2 DSC curves of BBCP/LiTf samples of r = 0, 0.05, 0.1, and 0.5 (The unfilled cycles indicate T_g; Inset: T_g versus r for PEO (○) and PS (□), and T_g of PEO/LiTFSI mixture (▲) for comparison.)

became wider at low doping (r = 0.05 and 0.1), while narrower at high doping (r = 0.5). Along with the segregation, T_gs of PEO and PS increased with the salt contents, seen more clearly in the inset. The increase tendency of $T_{g,PEO}$ versus r (circle symbols) was similar to that of PEO/lithium salt mixtures (triangle symbols)[34, 35]. On the other hand, the increase tendency of $T_{g,PS}$ versus r (square symbols) was attributed to a stronger PEO/PS segregation at higher salt content, because T_g approaches gradually to that of PS homopolymer with increasing r. $T_{g,PEO}$s of the lithium-doped BBCP was systematically larger than those of PEO/LiTFSI, partly due to incomplete segregation of PEO from high $T_{g,PS}$, which will be discussed later. The incompletely segregated structures suppress the crystallization of PEO domains, which is also verified from the results of wide angle X-ray scattering measurement (Fig. S8, in ESI). No scattering peak is seen from the curves.

SAXS and TEM experiments were carried out to investigate the morphology of the BBCP doped with LiTf. Figure 3(a) shows the SAXS intensity $I(q)$ plotted against q. The raw $I(q)$ data were shifted vertically by multiplying a factor to avoid overlapping. Since a change of $I(q)$ with temperature is trivial, $I(q)$ is only shown at two boundary temperatures of the measurement, *i.e.* room temperature and 140 °C. For BBCP without lithium salt, the lack of a scattering peak suggests molecular-scale miscibility for the PEO and PS side chains, in accordance with the DSC results and no structural feature in the TEM image. When doped with lithium salt with r = 0.05, the SAXS curve shows only one wide peak, indicating weak microphase segregation. The peak becomes sharper and shifts to lower q as r increases to 0.1, indicating a stronger microphase separation. Absence of higher order peaks suggests no ordered structure formed. A scattering peak at q^* = 0.615 nm^{-1} gives a domain spacing of $d = 2\pi/q^*$ = 10.2 nm. This spacing is not clearly seen in the TEM image, where only randomly distributed black dots appear, which should correspond to the PEO condensed regions stained by RuO_4. The PEO brushes are partly segregated, as schematically shown in the inset of Fig. 3(c).

For r = 0.5, a sharp large peak and several higher order peaks with scattering vector ratios of 1:2:3 appear. This is indicative of a lamellar morphology, which is confirmed by TEM image (Fig. 3b). The higher order peaks are weak in SAXS and phase boundaries are unclear in TEM, both

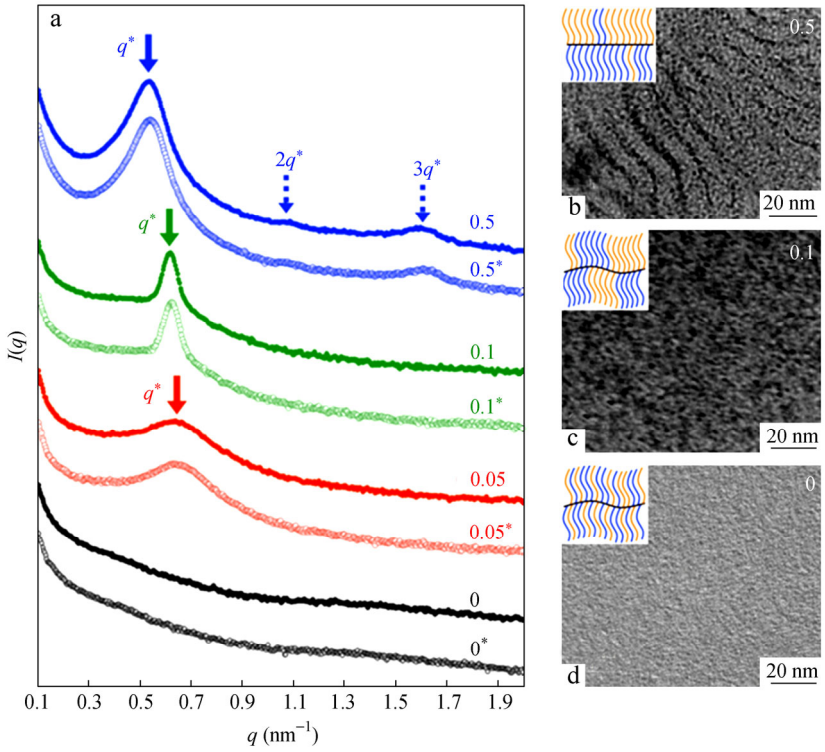

Fig. 3 SAXS curves of BBCP/LiTf samples of r = 0, 0.05, 0.1, and 0.5 at room temperature (marked with star) and 140 °C (a); TEM images for r = 0.5 (b), 0.1 (c), and 0 (d) (The insets are schematic representations of the BBCP conformation.)

https://doi.org/10.1007/s10118-018-2016-z

suggesting incomplete phase separation even at this high salt loading, as schematically shown in the inset of Fig. 3(b). The d-space of the lamellae calculated from SAXS is d = 11.7 nm, in accordance with that seen in TEM image. To understand the d-spacing, we make a rough estimation. The volume occupied by one macromonomer can be estimated as $V_X = m_X/(\rho_X N_{AV})$, with X = PS or PEO. Here, ρ is the density (ρ_{PS} = 0.97 g/cm^3 and ρ_{PEO} = 1.06 g/cm^3) and N_{AV} the Avogadro number. The calculation gives V_{PS} = 5.0 nm^3 and V_{EO} = 1.5 nm^3. Since LiTf is selectively located in PEO phase, the volume of the salts corresponding to each PEO macromonomer is $V_{LiTf} = r \times n_{PEO} M_{LiTf}/(\rho_{LiTf} N_{AV})$ = 1.4 nm^3, where n_{PEO} (= 20) is the number of repeat units per PEO brush, M_{LiTf} = 156 g/mol and ρ_{LiTf} = 1.9 g/cm^3. The volume occupied by one macromonomer on average would be $V = f_{PS}V_{PS} + f_{PEO}(V_{PEO} + V_{LiTf})$ = 3.5 nm^3, with f_{PS} = 0.27 and f_{PEO} = 0.73, being the number fraction of PS and PEO brushes in BBCP. Assuming that the interchain distance in a direction perpendicular to the lamellar domain is the same as that parallel to the lamellar domain, this distance can be estimated as $d = 2(V/2l)^{1/2}$ = 8.4 nm, with l = 0.1 nm being the length of each backbone bond. This estimated distance is in reasonable agreement with the SAXS result. The assumption is acceptable, *i.e.* side chains are equally stretched in both directions (perpendicular and parallel to the lamellar domain). The thickness of the PS and PEO domain can be estimated as $D_{PS} = df_{PS}V_{PS}/V$ = 4.6 nm and $D_{PEO} = df_{PEO}(V_{PEO} + V_{LiTf})/V$ = 7.1 nm. On the other hand, the mean end-to-end distance of the brush adopting Gaussian conformation can be estimated as $R_X = \{<R^2>/MM_X\}^{0.5}$ = 2.8 nm for X = PEO, and 3.6 nm for X = PS, with $<R^2>/M$ = 8.05 × 10^{-3} nm^2 for PEO and 4.34 × 10^{-3} nm^2 for PS[36] ($<R^2>$ represents the mean-square end-to-end distance and M means the molar mass.). R_{PS} (3.6 nm) < D_{PS} (4.6 nm) < 2R_{PS} (7.2 nm) means that PS side chains are neither strongly stretched nor strongly compressed to fill the PS domain. In comparison, D_{PEO} (7.1 nm) > 2R_{PEO} (5.6 nm) means that PEO side chains need to be stretched to fill the PEO domain uniformly[15].

Linear Viscoelasticity

The advantage of the binary brush structure is featured by PEO crystallization suppression and the mechanical strength enhancement. As described above, the PEO crystallization has been successfully suppressed. The mechanical strength enhancement is tested by linear viscoelasticity (LVE) measurement. In Fig. 4, the linear storage (G', unfilled symbols) and loss moduli (G'', filled symbols), measured at a single angular frequency ω = 1 rad/s in temperature sweep, are plotted against temperature for the samples with r = 0, 0.05, 0.1, and 0.5. Compared with the undoped sample, the moduli of the doped ones are highly increased. The storage moduli at room temperature are larger than 10^8 Pa, which should be high enough to suppress the dendrite growth. There are two main effects associated with the salt-induced segregation. The first one is that the T_g increases for both PS and PEO, which shifts their glassy moduli to higher temperature. No glassy modulus is detected in the experimental temperature range for BBCP bulk (r = 0). For r = 0.05 and 0.1, the T_gs of the PS microdomains appear at 55 and 75 °C, respectively. For r = 0.5, two glass transitions appear at 70 and 95 °C, which correspond to the glass transition of PEO and PS microdomains, respectively. These results are in accord with the DSC measurement.

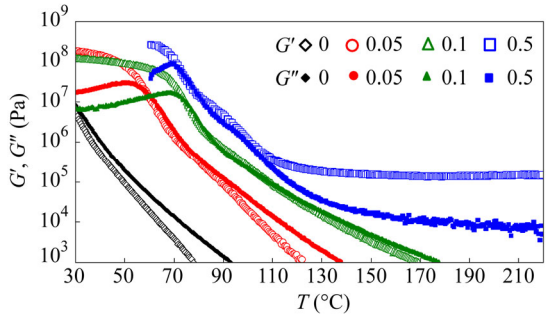

Fig. 4 Linear viscoelastic storage moduli G' (unfilled symbols) and loss moduli G'' (filled symbols), obtained as functions of temperature (T) for BBCP and the lithium doped BBCP with r = 0.05, 0.1, and 0.5

The second effect is the coordination between lithium ions and PEO segments, which is intensified with an increase in ion content[37–39]. In the rubbery modulus region (below 10^7 Pa), the storage moduli G' is much smaller than the loss moduli G'' for r = 0, 0.05, indicating a liquid like behavior therein. The sample of r = 0.1 shows very similar values of G' and G'', which reflects a close vicinity to the gel point. For r = 0.5, a clear rubbery plateau of ~10^5 Pa is seen, indicating a solid-like gel behavior. Thus, the system transfers from a typical liquid-like behavior to a solid-like behavior as the lithium doping amount increases. In order to further confirm the transition, we compared the linear viscoelastic moduli at the temperature 10–30 °C above the high temperature end of the glass transition region, where the storage moduli G' shows

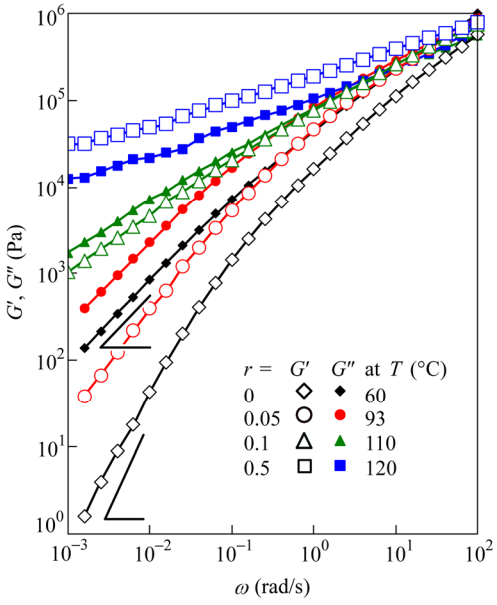

Fig. 5 Linear viscoelastic storage moduli G' (unfilled symbols) and loss moduli G'' (filled symbols) as function of angular frequency ω for the lithium doped BBCP with r = 0.05, 0.1, and 0.5 at indicated temperature

https://doi.org/10.1007/s10118-018-2016-z

similar values of ~10^6 Pa at ω = 100 rad/s (Fig. 5). The sol-to-gel transition is clearly seen: the terminals $G' \sim \omega^2$ and $G'' \sim \omega$ for r = 0 indicate a pure liquid behavior. $G' \approx G''$ for r = 0.1 reflects a close vicinity to the sol-gel transition point. $G' > G''$ for r = 0.5 means that the sample is already above the gel point[40].

Ionic Conductivity

The binary brush structure has positive effect on the ionic conductivity. Figure 6 compares the temperature dependence of DC conductivity σ_{DC} of the samples obtained from the DRS measurements, and that reported by Floudas and coworkers for the PEO/LiTf mixtures with M_n = 14000[41]. The σ_{DC} exhibits Vogel-Fulcher-Tammann (VFT)-type temperature dependence in a wide temperature range. The parameters are summarized in Table 1. In general, the conductivity decreases with increasing lithium doping ratio. It is related with the molecular architecture and the phase segregated structure induced by lithium ion. From the point of the polymer chain movement, the mobility of the lithium ions is limited due to T_g increase with increased lithium doping ratio. The incomplete phase segregation induced by lithium ion doping results in boundaries and defects in the nanodomains, as well as out of control of the orientation of the nanodomains. For r = 0.05, the liquid-like PEO domains in the weak microphase segregated structures facilitate ion conductivity, because the lithium ions migrate more easily between randomly dispersed, flexible PEO chains, compared to the well separated and stiff nanodomains. Another feature of the conductivity curves is that no abrupt transition of conductivity is seen as the function of temperature. For PEO/LiTf mixtures, in contrary, abrupt drops of conductivity are observed across PEO melting point ($1000/T > 3.0$) for all the lithium doping ratios. That is to say, the ionic conductivity at room temperature is low. We now focus on the r = 0.05 system, in which the crystallization of PEO (M_n = 14000) is successfully suppressed due to random introduction of PS brushes into BBCP. Therefore, the ionic conductivity at temperature below PEO melting point is higher than the reported data.

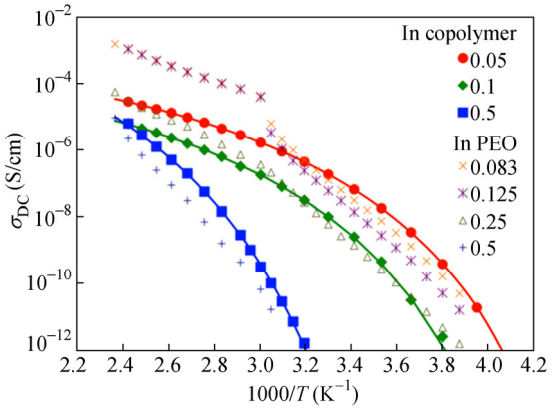

Fig. 6 DC conductivity σ_{DC} versus $1000/T$ for the BBCP/LiTf samples of r = 0.05, 0.1, and 0.5 (For comparison, the reported σ_{DC} data of PEO/LiTf mixtures are added[41]. Curves are fitted with VFT equation $\sigma_{DC} = \sigma_0 \exp[-B/(T - T_0)]$.)

Table 1 Structural and thermal data related with microphase separation of BBCP, and parameters related with the ion conductivity

[Li]/[EO] [a]	$T_{g,PEO}$ [b] (°C)	$T_{g,PS}$ [b] (°C)	T_0 [c] (°C)	σ_0 [c] (S/cm)	B [c]	$2\pi/q^*$ [d] (nm)
0	–43	15	–	–	–	–
0.05	–34	53	–73	0.0032	1000	9.7
0.1	–24	74	–63	0.0014	1100	10.2
0.5	61	92	–33	0.39	1900	11.7

[a] Lithium-doping ratio; [b] T_g of BBCP by DSC; [c] Calculated from fitting the conductivity with VFT equation $\sigma_{DC} = \sigma_0 \exp\{-B/(T - T_0)\}$; [d] q^* is the scattering vector at the maximum scatting intensity from SR-SAXS curves.

CONCLUSIONS

We have synthesized random binary brush block copolymers containing PS and PEO brushes. The introduction of PS brushes influences the behavior of PEO in morphology, viscoelasticity and the ionic conductivity. Due to the random feature of the brushes, PEO crystallinity is successfully suppressed. This is the key factor that the doped BBCP has high ionic conductivity at room temperature. Meanwhile, the PS brushes provide mechanical support for PEO domains. The storage moduli of the lithium doped BBCP are larger than 10^8 Pa at room temperature, which are high enough to suppress the dendrite growth. Therefore, the lithium doped BBCP exhibits both high ionic conductivity and high mechanical strength at room temperature. Further exploitation of the system is currently under investigation.

Electronic Supplementary Information

Electronic supplementary information (ESI) is available free of charge in the online version of this article at http://dx.doi.org/10.1007/s10118-018-2016-z.

ACKNOWLEDGMENTS

L.C.G. is grateful for financial support from the National Key Research and Development Program of China (2017YFA0206904, 2017YFA0206900). Q.C. is grateful for start-up fund of Changchun Institute of Applied Chemistry, Chinese Academy of Sciences. We thank Dr Ralph Colby at Penn. State Univ. for helpful comments.

REFERENCES

1 Manuel, S. A. Review on gel polymer electrolytes for lithium batteries. Eur. Polym. J. 2006, 42(1), 21–42.
2 Tarascon, J. M.; Armand, M. Issues and challenges facing rechargeable lithium batteries. Nature 2001, 414(6861), 359–367.
3 Fenton, D. E.; Parker, J. M.; Wright, P. V. Complexes of alkali metal ions with poly(ethylene oxide). Polymer 1973, 14(11), 589–589.
4 Patel, S. N.; Javier, A. E.; Stone, G. M.; Mullin, S. A.; Balsara, N. P. Simultaneous conduction of electronic charge and lithium ions in block copolymers. ACS Nano 2012, 6(2), 1589–1600.
5 Yang, L. Y.; Wei, D. X.; Xu, M.; Yao, Y. F.; Chen, Q. Transferring lithium ions in nanochannels: a PEO/Li^+ solid polymer electrolyte design. Angew. Chem. Int. Ed. 2014, 53(14), 3631–3635.
6 Vöge, A.; Deimede, V.; Paloukis, F.; Neophytides, S. G.; Kallitsis, J. K. Synthesis and properties of aromatic polyethers containing poly(ethylene oxide) side chains as polymer electrolytes for lithium ion batteries. Mater. Chem. Phys. 2014, 148(1-2), 57–66.

7 Sinha, K.; Maranas, J. Does ion aggregation impact polymer dynamics and conductivity in PEO-based single ion conductors? Macromolecules 2014, 47(8), 2718–2726.
8 Gao, S.; Zhong, J.; Xue, G.; Wang, B. Ion conductivity improved polyethylene oxide/lithium perchlorate electrolyte membranes modified by graphene oxide. J. Membr. Sci. 2014, 470, 316–322.
9 Sun, J.; Stone, G. M.; Balsara, N. P.; Zuckermann, R. N. Structure-conductivity relationship for peptoid-based PEO-mimetic polymer electrolytes. Macromolecules 2012, 45(12), 5151–5156.
10 Christie, A. M.; Lilley, S. J.; Staunton, E.; Andreev, Y. G.; Bruce, P. G. Increasing the conductivity of crystalline polymer electrolytes. Nature 2005, 433(7021), 50–53.
11 Xiao, Q.; Wang, X.; Li, W.; Li, Z.; Zhang, T.; Zhang, H. Macroporous polymer electrolytes based on PVDF/PEO-*b*-PMMA block copolymer blends for rechargeable lithium ion battery. J. Membr. Sci. 2009, 334(1-2), 117–122.
12 Song, J. J.; Wang, Y. Y.; Wan, C. C. Review of gel-type polymer electrolytes for lithium ion batteries. J. Power Sources 1999, 77(2), 183–197.
13 Fontenella, J. J.; Wintergill, M. C.; Calame, J. P.; Andeen, C. G. Electrical relaxation in pure and alkali metal thiocynate complexed with poly(ethylene oxide). Solid State Ionics 1983, 8(4), 333–339.
14 Chen, H. W.; Chang, F. C. The novel polymer electrolyte nanocomposite composed of poly(ethylene oxide), lithium triflate and mineral clay. Polymer 2001, 42(24), 9763–9769.
15 Panday, A.; Mullin, S.; Gomez, E. D.; Wanakule, N.; Chen, V. L.; Hexemer, A.; Pople, J.; Balsara, N. P. Effect of molecular weight and salt concentration on conductivity of block copolymer electrolytes. Macromolecules 2009, 42(13), 4632–4637
16 Singh, M.; Odusanya, O.; Wilmes, G. M.; Eitouni, H. B.; Gomez, E. D.; Patel, A. J.; Chen, V. L.; Park, M. J.; Fragouli, P.; Iatrou, H.; Hadjichristidis, N.; Cookson, D.; Balsara, N. P. Effect of molecular weight on the mechanical and electrical properties of block copolymer electrolytes. Macromolecules 2007, 40(13), 4578–4585.
17 Stone, G. M.; Mullin, S. A.; Teran, A. A.; Hallinan, D. T.; Minor, A. M.; Hexemer, A.; Balsara, N. P. Resolution of the modulus versus adhesion dilemma in solid polymer electrolytes for rechargeable lithium metal batteries. J. Electrochem. Soc. 2012, 159(3), A222–A227.
18 Choi, S.; Cho, B. K. Liquid crystalline and ion-conducting properties of mesogenic dendron-coil-dendron copolymers: characterization of LC phases using normalized conductivity. Soft Matter 2013, 9(16), 4241-4248.
19 Inceoglu, S.; Rojas, A. A.; Devaux, D.; Chen, X. C.; Stone, G. M.; Balsara, N. P. Morphology-conductivity relationship of single-ion-conducting block copolymer electrolytes for lithium batteries. ACS Macro Lett. 2014, 3(6), 510–514.
20 Shi, J.; Vincent, C. A. The effect of molecular weight on cation mobility in polymer electrolytes. Solid State Ionics 1993, 60(1-3), 11–17.
21 Money, B. K.; Hariharan, K.; Swenson, J. Glass transition and relaxation processes of nanocomposite polymer electrolytes. J. Phys. Chem. B 2012, 116(26), 7762–7770.
22 Xia, Y.; Olsen, B. D.; Kornfield, J. A.; Grubbs, R. H. Efficient synthesis of narrowly dispersed brush copolymers and study of their assemblies: the importance of side chain arrangement. J. Am. Chem. Soc. 2009, 131(51), 18525–18532.
23 Ruzette, A. V. G.; Soo, P. P.; Sadoway, D. R.; Mayes, A. M. Melt-formable block copolymer electrolytes for lithium rechargeable batteries. J. Electrochem. Soc. 2001, 148(6), A537–A543.
24 Gao, L. C.; Zhang, C. L.; Liu, X.; Fan, X. H.; Wu, Y. X.; Chen, X. F.; Shen, Z.; Zhou, Q. F. ABA type liquid crystalline triblock copolymers by combination of living cationic polymerizaition and ATRP: synthesis and self-assembly. Soft Matter 2008, 4(6), 1230–1236.
25 Xue, B.; Gao, L.; Jiang, H.; Geng, Z.; Guan, S.; Wang, Y.; Liu, Z.; Jiang, L. High flux CO_2 transporting nanochannel fabricated by self-assembly of linear-brush block copolymer. J. Mater. Chem. A 2013, 1(28), 8097–8100.
26 Chung, G.; Kornfield, J.; Smith, S. Component dynamics miscible polymer blends: a two-dimensional deuteron NMR investigation. Macromolecules 1994, 27(4), 964–973.
27 Chung, G. C.; Kornfield, J.; Smith, S. Compositional dependence of segmental dynamics in a miscible polymer blend. Macromolecules 1994, 27(20), 5729–5741.
28 Lodge, T. P.; McLeish, T. C. Self-concentrations and effective glass transition temperatures in polymer blends. Macromolecules 2000, 33(14), 5278–5284.
29 Kumar, S. K.; Colby, R. H.; Anastasiadis, S. H.; Fytas, G. Concentration fluctuation induced dynamic heterogeneities in polymer blends. J. Chem. Phys. 1996, 105(9), 3777–3788.
30 Nakamura, I.; Balsara, N. P.; Wang, Z. G. First-order disordered-to-lamellar phase transition in lithium salt-doped block copolymers. ACS Macro Lett. 2013, 2(6), 478–481.
31 Nakamura, I.; Balsara, N.; Wang, Z. G. Thermodynamics of ion-containing polymer blends and block copolymers. Phys. Rev. Lett. 2011, 107(19), 198301.
32 Nakamura, I.; Wang, Z. G. Salt-doped block copolymers: ion distribution, domain spacing and effective parameter. Soft Matter 2012, 8(36), 9356–9367.
33 Ren, C. L.; Nakamura, I.; Wang, Z. G. Effects of ion-induced cross-linking on the phase behavior in salt-doped polymer blends. Macromolecules 2016, 49(1), 425–431.
34 Vachon, C.; Labreche, C.; Vallee, A.; Besner, S.; Dumont, M.; Prud'Homme, J. Microphase separation and conductivity behavior of poly(propylene oxide)-lithium salt electrolytes. Macromolecules 1995, 28(16), 5585–5594.
35 Lemaı, F.; Prud'homme, J. Ion-ion, short-range interactions in PEO-LiX rubbery electrolytes containing LiSCN, $LiN(CF_3SO_2)_2$ or $Li[CF_3SO_2N(CH_2)_3OCH_3]$ as deduced from studies performed on PEO-LiX-KX ternary systems. Electrochim. Acta 2001, 46(9), 1359–1367.
36 Fetters, L.; Lohse, D.; Colby, R. in "Physical Properties of Polymers Handbook", Springer, 2007, p. 447–454.
37 Staunton, E.; Christie, A. M.; Martin-Litas, I.; Andreev, Y. G.; Slawin, A. M.; Bruce, P. G. Structure of the poly (ethylene oxide)-zinc chloride complex. Angew. Chem. Int. Ed. 2004, 116(16), 2155–2157.
38 Matsumiya, Y.; Balsara, N. P.; Kerr, J. B.; Inoue, T.; Watanabe, H. *In situ* dielectric characterization of poly(ethylene oxide) melts containing lithium perchlorate under steady shear flow. Macromolecules 2004, 37(2), 544–553.
39 Goldansaz, H.; Auhl, D.; Goderis, B.; Voleppe, Q.; Fustin, C. A.; Gohy, J. F.; Bailly, C.; van Ruymbeke, E. Transient metallo-supramolecular networks built from entangled melts of poly(ethylene oxide). Macromolecules 2015, 48(11), 3746–3755.
40 Winter, H. Can the gel point of a cross-linking polymer be detected by the G'-G'' crossover? Polym. Eng. Sci. 1987, 27(22), 1698–1702.
41 Zardalidis, G.; Ioannou, E.; Pispas, S.; Floudas, G. Relating structure, viscoelasticity, and local mobility to conductivity in PEO/LiTf electrolytes. Macromolecules 2013, 46(7), 2705–2714.

https://doi.org/10.1007/s10118-018-2016-z